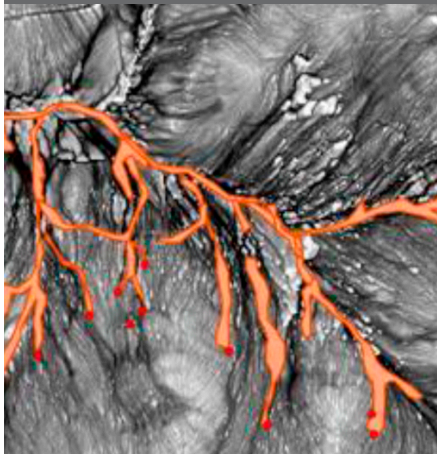


**Special Section:
Preferential Flow**

Adrian A. Harpold*
Steve W. Lyon
Peter A. Troch
Tammo S. Steenhuis



This study attempted to determine the sources of stream runoff in a watershed. Field measurements suggested that hillside saturated areas connected to the stream during rain events via lateral preferential flowpaths. The lateral flow paths reduced the influence of surface topography and channel topology on sources of stream runoff.

A.A. Harpold and T.S. Steenhuis, Dep. of Biological and Environmental Engineering, Cornell Univ., Ithaca, NY 14853; S.W. Lyon, Physical Geography and Quaternary Geology, Stockholm Univ., Stockholm, Sweden; A.A. Harpold and P.A. Troch, Hydrology and Water Resources, Univ. of Arizona, Tucson, AZ; P.A. Troch, Biosphere 2 Earth Science, Univ. of Arizona, Tucson, AZ. *Corresponding author (aharpold@email.arizona.edu).

Vadose Zone J. 9:397–414
doi:10.2136/vzj2009.0107
Received 16 July 2009.
Published online 3 May 2010.

© Soil Science Society of America
5585 Guilford Rd. Madison, WI 53711 USA.
All rights reserved. No part of this periodical may be reproduced or transmitted in any form or by any means, electronic or mechanical, including photocopying, recording, or any information storage and retrieval system, without permission in writing from the publisher.

The Hydrological Effects of Lateral Preferential Flow Paths in a Glaciated Watershed in the Northeastern USA

Despite observational evidence of lateral preferential flow paths in northeastern U.S. watersheds, their effects on the sources of runoff remain unclear. An intense field survey was undertaken during the 2007 growing season to determine the sources of stream runoff from a 2.51 km² watershed in the Catskill Mountains, New York State. Lateral preferential flow paths are caused by groundwater springs and soil piping in this region. A two-component hydrograph separation using $\delta^{18}\text{O}$ showed that event water (rain water) was a significant source of runoff during nine rainfall events (from July to October). With these rainfall events, 14 to 37% of the volume and 18 to 49% of the peak streamflow was attributable to event water. Further, end-member mixing analysis (EMMA), using $\delta^{18}\text{O}$, Si, and dissolved organic carbon (DOC), showed that saturated areas accounted for 2 to 24% of the total volume and 4 to 59% of peak streamflow but that groundwater was the dominant source of runoff volume during all events. Field surveys of saturated areas also suggested that near-stream areas were insufficient to generate the observed stream chemistry during rainfall events larger than 8 mm. A connection with the hillside saturated areas was therefore required to explain the results of the hydrograph separations, which were corroborated by the timing of the transient (perched) groundwater and overland flow. The hydrometric measurements confirmed that hillside lateral preferential flow paths rapidly transported water to near-stream saturation areas during runoff events under relatively dry antecedent conditions. A qualitative comparison with conventional techniques for distributing variable saturation areas (VSA) using surface topography and soil transmissivity (i.e., topographic index and soil topographic index), which do not consider the effects of lateral preferential flow paths, demonstrated that typical parameterizations (on the order of $<10^{-1}$ m) would not have the spatial resolution to represent the measured lateral preferential flow paths (on the order of $<10^{-3}$ m). Overall, the results suggest that the lateral redistribution of water from hillside areas reduces the influence of surface topography and channel topology on the sources of stream runoff, a finding that is consistent with recent ones from other landscapes where glacial soils have coevolved with the terrestrial hydrology.

Abbreviations: DEM, Digital Elevation Model; DOC, dissolved organic carbon; EMMA, end-member mixing analysis; GPS, global positioning system; NRCS, Natural Resource Conservation Service; NSGW, near-stream groundwater; PCA, principal component analysis; PGW, permanent groundwater; SP1, spring 1; SP2, spring 2; SP3, spring 3; SPO, soil pipe outlet; SSURGO, Soil Survey Geographic; STI, soil topographic index; TGW1, transient groundwater (valley bottom); TGW2, transient groundwater (hillside); TI, topographic index; VSA, variable saturation areas; VSMOW, Vienna Standard Mean Ocean Water.

The spatiotemporal characterization of hydrological flow paths resulting from complex subsurface heterogeneities is fundamental to modeling catchment hydrology and water quality (Lin, 2006; Beven and Feyer, 2002). Still, many contemporary models are based on conventional theories (such as Darcy's Law, the advection-dispersion equation, and conservation of mass) implying that water and solutes move within a small deviation of an average (advective) velocity. To account for both the long- and short-term memory (Kirchner et al., 2000) found in real hydrologic systems using these conventional theories would require the explicit mapping of all the heterogeneous subsurface properties. This is practically an impossible task even in small research watersheds (Beven and Feyer, 2002; McDonnell et al., 2007). Most models instead rely on implicit calibration to account for a lack of knowledge about spatial heterogeneities (particularly in the subsurface) (McDonnell et al., 2007). However, there is concern that models calibrated to the outlet response may not be correctly capturing the internal processes of the watershed that are critical for soil and water management. McDonnell et al. (2007) therefore suggest that simple explanations for the emergence, maintenance, and interconnections of landscape heterogeneities could have widespread implications for improving hydrologic and transport

models. Although their work points toward a new approach, simple and generalizable explanations for internal processes in ungauged basins still remain elusive because of the incredible variety in observed watershed responses (Troch et al., 2008).

Some common principles are emerging for predicting dominant runoff processes in ungauged watersheds by comparing watersheds across landscape units (e.g., McGlynn et al., 2004), spatial scales (e.g., McGuire et al., 2005; Hrachowitz et al., 2009), and geomorphologic provinces (e.g., Tetzlaff et al., 2009). It is generally accepted, for example, that in steep terrain, gravitationally driven subsurface flow paths dominate and surface topography is more important than catchment size in determining average hydrologic response (Tetzlaff et al., 2009; McGuire et al., 2005). The channel drainage network (topology) is also an important hydrologic control in watersheds where landscape features adjacent to the stream are important sources of runoff (Buttle, 2006; McGlynn et al., 2004) and at larger spatial scales, where in-stream transit times are significant. However, Buttle (2006) proposed that a third control, namely, runoff typology, needs to be considered in addition to surface topography and channel topology for watersheds with heterogeneous subsurface properties.

When sections of the landscape partition water differently between lateral and vertical movement (i.e., runoff typology), the effects of subsurface properties become increasingly important. For example, the runoff typology of the Cairngorms Mountains, Scotland, is radically different between the highly responsive peat soils, where water is transported laterally by overland flow, and the more free-draining podzolic soils, where vertical flow dominates (Soulsby et al., 2006; Soulsby and Tetzlaff, 2008; Hrachowitz et al., 2009). As a consequence, Soulsby et al. (2006) could show that, even at a basin scale of 230 km^2 , differences in runoff typology at the hillslope scale reduce the influence of the surface topography and channel topology. The work in the Cairngorms demonstrates how differences in runoff typography (vertical versus lateral runoff partitioning) can alter the flow paths and source areas in landscapes with complex glacial soils.

The landscape in the glaciated northeastern United States is composed of hillsides and uplands with shallow, highly permeable soils and of valley bottoms with deeper, poorly drained soils. Clear differences in runoff typography occur between VSA that are dominated by lateral runoff and areas of deep drift and alluvial deposits that are more freely draining. Saturation-excess runoff from VSA is the dominant runoff mechanism (Betson, 1964; Dunne and Black, 1970; Dunne et al., 1975), and high infiltration rates make infiltration-excess runoff unlikely during storms (Walter et al., 2002). The spatial distribution of VSA is in part driven by topography, which causes saturation in flatter areas, at breaks in slope, or where upslope contributing areas are large (Beven and Kirkby, 1979). The classical conceptualization of VSA dynamics predicts that VSA will develop in the areas adjacent to the stream channel

(Dunne et al., 1975; Engman, 1974), making the channel topology important where the subsurface heterogeneities are minor. Not surprisingly, models derived from these conceptualizations have focused on topographic surface controls on VSA and, as such, may be neglecting the role of subsurface heterogeneities in these complex glacial landscapes.

Distributed VSA models are routinely calibrated with watershed discharge to predict runoff source areas for soil and water management, but a lack of validation with measured spatial data means that we may not be “getting the right answers for the right reasons” (Beven and Feyen, 2002). Potential weaknesses in the predictions from VSA models could result from the following: (i) a lack of spatial detail that allows for adequate representation in the soil and topographic input information, (ii) a partial process understanding that may not include all relevant mechanisms or both. Regardless of these potential weaknesses, the conceptual understanding of the connection between VSA and runoff volumes has been well established by Steenhuis et al. (1995). That work convincingly showed that discharge could be adequately predicted by a distribution of soil storages where just part of a watershed’s soils reach field capacity (the VSA extent) and lead to runoff generation. The disadvantage of this approach is that it does not explicitly map the distribution of storages in the watershed; thus, models are commonly used to predict VSA locations based on the topographic index (TI) (Beven and Kirkby, 1979) and the soil topographic index (STI) (Ambroise et al., 1996), which are based on local slope, upslope area, and soil transmissivity. Further, these spatial indices can be parameterized to develop distributed models that predict the spatiotemporal sources of runoff during rainfall events across various antecedent conditions (e.g., Mehta et al., 2004; Lyon et al., 2004; Dahlke et al., 2009). A shortcoming is that these models are strongly reliant on accurate topographic and soils information and are limited to treating grid cells (typically 10 by 10 m) as homogenous units. The existence of lateral preferential flow paths potentially highlights the weaknesses in this current generation of VSA models. First, such lateral preferential flow paths are not considered explicitly in model structures. Second, the lateral preferential flow paths and their associated hydrologic processes may act at spatial scales much finer than those typically considered in most VSA models.

The influence of lateral preferential flow paths on the spatial extent of VSA is limited because of a lack of field-scale investigations. Several previous studies have observed that water was supplied to near-stream saturated areas from subsurface macropores (Waddington et al., 1993; Buttle and Peters, 1997), and overland flow from upslope groundwater springs (Engman, 1974; Inamdar and Mitchell, 2007). Dunne et al. (1975) and Dunne and Black (1970) showed that during wet conditions in Sleepers River, Vermont, the saturated areas and overland flow were controlled by the location of groundwater seeps. Subsurface lateral preferential flow paths also act along perched water tables on restrictive

layers (Lin, 2006; Lin and Zhou, 2008) and along the bedrock-soil interface (Tromp-van Meerveld and McDonnell, 2006), which can connect to the stream or near-stream VSA during larger runoff events. Overall, these lateral preferential flow paths act to change the runoff typography across the landscape by increasing lateral flow, thereby reducing the influence of surface topography and channel network topology on runoff sources. The inclusion of lateral preferential flow paths in VSA models therefore has the potential to improve the runoff predictions used to make management decisions.

The goal of this study was to determine the importance of hillside lateral preferential flow paths in the spatial distribution of runoff sources during rainfall events under relatively dry growing-season conditions. The study was performed in the Catskill Mountains, New York State, where several preferential flow paths (e.g., soil pipes and groundwater springs) have been located and monitored. Intensive in-field monitoring was used to map the extent of saturated areas in the landscape and their hydrologic connectivity. The contributions of saturated areas to stream runoff were investigated using a combination of hydrometric, chemical, and isotopic measurements during nine growing-season storm events (July to October). The findings of this study are intended to help better define basic watershed functioning and to improve the characterization of complex lateral flow paths in this glaciated, mixed-use watershed, which is representative of those found in the northeastern USA.

Materials and Methods

Study Site

The 60-ha study hillslope is part of a 2.51-km² study watershed in the southwest corner of the 36.5-km² Town Brook watershed in the Catskill Mountain region of New York State (Fig. 1). The study watershed was cleared for grazing in the early eighteenth century but has returned to 75% forest that is dominated by hardwoods such as American beech (*Fagus grandifolia* Ehrh.), red maple (*Acer rubrum* L.), sugar maple (*Acer saccharum* Marsh.), and yellow birch (*Betula alleghaniensis* Britton) (Kurdish, 2002), and 25% shrub and brush (Fig. 1). Watershed elevation ranges from 585 m to 935 m, with slopes from 0° to 40°. Climate is characteristically humid, with an average annual temperature of 8°C and average annual precipitation of about 900 mm.

The Catskill Mountains have characteristic glacial features typical of watersheds in the northeastern United States. Sandstones (60%) and interbedded siltstones and shales (40%) produce contact springs on the hillsides (Rich, 1934; Reynolds, 2000). Soil development has been highly influenced by glacial features, with

deep drift features in the valley bottoms and shallow, undeveloped till soils on the hillsides. Effective soil depths are limited by a compacted restrictive layer, referred to as a fragipan, at 30 and 70 cm depths across most of the hillslope (USDA, 2007). The effective conductivity of the fragipan is roughly 0.5 cm h⁻¹, or an order of magnitude less than that of the well-drained surface material (15 cm h⁻¹) (USDA, 2007).

The catena at the study hillslope is derived from glacial till composed from reddish sandstone, siltstone, and shale. The soils are all silt loam with high (>10%) proportions of rock fragments, and consist of 35% Willowmoc soils, 30% Lackawanna soils, 10% Onteora soils, and 25% soils of minor extent (USDA, 2007). The Lackawanna soils are on the hillsides and convex hilltops and have a moderately draining layer above the dense fragipan (Fig. 1). The Willowmoc soils are located slightly down the hillsides and also have moderately draining surface layers (Fig. 1). The Onteora soils, in the flat valley bottoms (Fig. 1), have a much lower transmissivity. The soil maps were developed from Soil Survey Geographic (SSURGO) data along with associated attribute tables (Map Unit Identification Records), which are used to determine soil properties (USDA, 2007). The SSURGO data is the most detailed soil mapping done by the Natural Resource Conservation Service (NRCS), having resolutions between 1:12,000 and 1:63,630 (USDA, 2007).

Field Collection

Water chemistry and quantity measurements were made at a variety of locations during the growing season of 2007. Water-table heights were measured at four locations (Fig. 1) using WT-HR 500 and 1000 capacitance probes (TruTrack, Christchurch, New

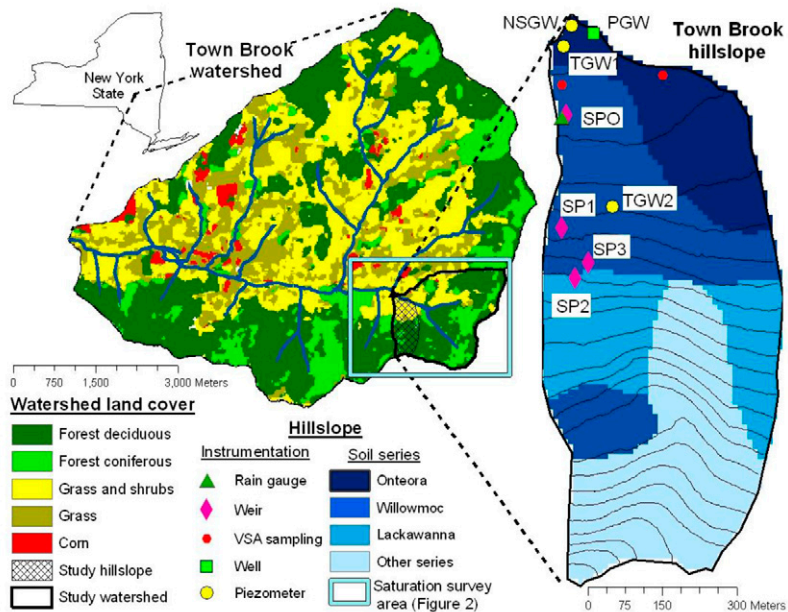


Fig. 1. Measurements locations in the southeast corner of Town Brook watershed, a mixed land-use watershed in the Catskill Mountains. Hillslope measurements were made at four well locations, four weirs, a rain gauge, and two saturated areas during nine storm events. Soils are composed of several classification series across the hillslope.

Zealand)¹ inside 2.5-cm PVC tubes and screened to various depths. Measurements were made at different positions along the hillslope to capture transient groundwater response above the fragipan layer and to capture the deeper permanent groundwater response. The permanent groundwater (PGW) measurement was made about 1.0 m from the stream at a location without a fragipan layer using a well that was screened from 0.2 m to 0.6 m from the surface. The remaining three piezometers measured the transient groundwater with a screen 5 cm above the fragipan to various depths: in the near-stream at a depth of 50 cm (NSGW), in the low-angle valley bottom at a depth of 55 cm (TGW1), and on the steeper hillside at a depth of 40 cm (TGW2). Sand was deposited at the bottom 25 cm of the well and at the bottom 5 cm of piezometers. Native soils (without rock fragments) were used to backfill to the surface. Water table depths were measured at 15-min intervals during the rainfall events.

Overland flow discharge measurements were also made at four locations (Fig. 1). In the areas with continuous baseflow, spring 1 (SP1) and the soil pipe outlet (SPO), H-flumes were installed. At the other two more transient, overland flow locations, spring 2 (SP2) and spring 3 (SP3), Parshall flumes were installed. Overland flow was too diffuse just below the spring outlets to install the flumes; thus, the installation was made approximately 5 to 10 m below the spring outlet, leaving a small saturated area above some of the flumes (see the next paragraph). Discharge data was collected every 15 min using Druck water-level pressure transducers (model GB PTX 1830, GE Sensing, Billerica, MA) connected to Telog data recorders (Telog Instruments, Victor, NY). Stage-discharge relationships were developed for the flumes across a range of discharges.

The extent of saturated areas was measured using a global positioning system (GPS) unit and intensive field surveys. The soil was determined to be saturated using the boot-print technique, that is, by making a small depression (1 to 2 cm) in the soil and observing if it refilled with water. The GPS had an accuracy of 3 m or better during the surveys and was subsequently uploaded into a geographic information systems program to calculate the spatial coverage. Errors in these estimates could result from small ($<5 \text{ m}^2$) saturation areas that were missed or not well represented by the GPS measurements. As a result, more detailed surveys with measuring tapes were made at the small saturation areas above the weirs of SP1, SP2, and SP3 across a range of conditions. The extent of saturated area above SP2 varied from approximately 0 to about 16 m^2 and at SP3, from approximately 2 to about 19 m^2 . Continuous baseflow discharge at SP1 created a larger saturation area of approximately 5 to 24 m^2 . The SPO also maintained discharge during the driest summer periods, presumably from water transported on top of the dense fragipan layer, and thus did not have an attributable upslope saturated area.

¹ The use of brand names in this paper is for identification purposes only.

Water chemistry was also monitored at a variety of locations across the watershed. Grab samples were collected from the stream at 15-min intervals using an ISCO automatic water sampler (Teledyne Isco, Lincoln, NE) mounted 5 cm above the channel bed. Rainwater was collected 0.5 m from the ground surface near the tipping bucket (Fig. 1) and at a forested location below the canopy. Rainwater was collected in 2-mm increments and mixed between the two 30-cm funnel collectors proportionately to the volume collected. Soil water was collected using free-draining lysimeters that were installed perpendicular to the face of a soil pit adjacent to the NSGW location (Fig. 1) at depths of 15 and 40 cm. The lysimeters were made from 5-cm PVC pipes that were backfilled with sand and gravity-fed to a collection vessel in the bottom of the covered soil pit, which was pumped after the storm events. The volume of water collected from each lysimeter was considered indicative of the amount of flow through the soil horizon, which was minimal ($<30 \text{ mL}$) in the largest events and did not occur in five of the nine events. Water samples from saturation areas were mixed from two locations (Fig. 1) and sampled at the water surface to minimize the amount of particulate organic matter collected. Near-stream groundwater samples were collected before and during each event from the observation well located 1 m from the stream (Fig. 1). Spring water was sampled during baseflow from weirs located 5 to 10 m from the spring outlet.

The TI (Beven and Kirkby, 1979) and STI (Ambroise et al., 1996) were employed to capture the overall dynamics of saturated extent based on topography and soils. The TI was calculated based on the Digital Elevation Model (DEM):

$$\text{TI} = \frac{\alpha}{\tan\beta} \quad [1]$$

where α is the upslope contributing area (m^2) and β is the local surface topographic slope (radians). Large TI values mean that areas receive more upslope water or are less steep or both. The STI was calculated from a DEM and soil properties given in the SSURGO soil survey data:

$$\text{STI} = \frac{\alpha}{DK_s \tan\beta} \quad [2]$$

where D is the local soil depth (m) and K_s the saturated hydraulic conductivity (md^{-1}). Large STI values indicate locations that are more prone to saturation.

Laboratory Analysis

All samples were refrigerated until analyzed. Major ions and DOC were analyzed in the Soil and Water Laboratory in the Biological Environmental Engineering Department at Cornell University. The water samples were first passed through a 0.45 μm nitrocellulose filter. The cations Si and Ca were then analyzed with a Thermo Jarrel Ash inductively coupled plasma spectrometer with

a customized axial-view torch and reported to within a 15% error. The anion Cl was analyzed with the Dionex ICS-2000 (Dionex, Sunnyvale, CA) with an anion column and reported to within a 10% error. The DOC was measured with the OI Analytical 1010 wet oxidation TOC/DOC analyzer (OI Analytical, College Station, TX) with a 10% error and a 10% coefficient of variation.

The $\delta^{18}\text{O}$ samples were stored in glass vials with polyseal caps to prevent evaporation and transported to the Laboratory of Isotope Geochemistry at the University of Arizona. All $\delta^{18}\text{O}$ samples were analyzed using a DLT-100 (model 908–0008, Los Gatos Research, Mountain View, CA) according to the methods outlined by Gehre et al. (1996) and were reported relative to Vienna Standard Mean Ocean Water (VSMOW) with a precision of 0.10% ($1 - \sigma$).

Hydrograph Separation Techniques

Three hydrograph separation techniques were used in this study: (i) quickflow (Hewlett and Hibbert, 1967), (ii) two-component isotopic separation (Sklash and Farvolden, 1979), and (iii) EMMA (Christopherson and Hooper, 1992). The hydrograph was separated into quickflow and delayed flow for each of nine storm events, as described by Hewlett and Hibbert (1967). A separation line was projected from the initial rise of the hydrograph at a slope of $0.5 \text{ s}^{-1} \text{ km}^{-2} \text{ h}^{-1}$. This method estimates the runoff ratio by dividing the quickflow by the rainfall amount for each event.

The two-component technique (Sklash and Farvolden, 1979) is a mass balance approach that separates the hydrograph into pre-event water (baseflow and water stored within the watershed before rainfall) and event water (rainwater) based on the stable isotope ratios:

$$Q_t C_t = Q_p C_p + Q_e C_e \quad [3]$$

where Q is discharge, C is the $\delta^{18}\text{O}$ VSMOW ‰ value, and the subscripts t, p, and e refer to total, pre-event, and event water, respectively. The contributions of event and pre-event water were estimated for each stream sample. The event water was estimated based on median $\delta^{18}\text{O}$ values of the rain samples collected at 2-mm increments. The pre-event water was the baseflow chemistry within 24 h of the beginning of the rain event. The uncertainty of each computed mixing fraction was evaluated using the technique described by Genereux (1998),

$$W_{fp} = \sqrt{\left[\frac{C_e - C_s}{(C_e - C_p)^2} W_{Cp} \right]^2 + \left[\frac{C_s - C_p}{(C_e - C_p)^2} W_{Ce} \right]^2 + \left[\frac{1}{(C_p - C_e)} W_{Ce} \right]^2} \quad [4]$$

where W_{fp} is the uncertainty of the pre-event mixing fraction, and W_{Cp} and W_{Ce} are the analytical uncertainties of the $\delta^{18}\text{O}$ values for pre-event and event water, respectively, and C_s is the $\delta^{18}\text{O}$ VSMOW ‰ value for stream water.

An EMMA model was used to estimate the runoff source areas following the steps outlined by Christopherson and Hooper (1992). First, linear plots of paired combinations of solutes (mixing diagrams) were used to find conservative tracers across all nine events. Second, the selected tracers were standardized into a correlation matrix such that solutes with greater variation did not exert more influence. Third, a principal component analysis (PCA) was completed for all combinations of three, four, and five solutes ($\delta^{18}\text{O}$, Si, DOC, Cl, and Ca). The selected model accounted for the greatest variability across all nine events using the three solutes $\delta^{18}\text{O}$, Si, and DOC with two principal components, implying that three end members (overland flow, throughfall, and groundwater) were necessary. The concentrations of the end members were then projected in the U-space that was defined by the stream PCA. The predicted tracer concentrations were evaluated using the least-squares linear regression. The EMMA model was then used to estimate the contributions from each of the three end members by solving the mass balance equations:

$$Q_{st} = Q_{of} + Q_{tf} + Q_{gw} \quad [5]$$

$$U1_{st} Q_{st} = U1_{of} Q_{of} + U1_{tf} Q_{tf} + U1_{tf} Q_{gw} \quad [6]$$

$$U2_{st} Q_{st} = U2_{of} Q_{of} + U2_{tf} Q_{tf} + U2_{tf} Q_{gw} \quad [7]$$

where Q_{st} is the stream discharge, $U1$ and $U2$ are the first and second components of PCA, and of, tf, and gw, correspond to the three end members: overland flow, throughfall (rainfall), and groundwater, respectively.

The uncertainty for each principal component was estimated using the method described by Burns et al. (2001) based on the analytical uncertainty of each solute:

$$W_{u,i} = \left[(V_{i,a} W_a)^2 + (V_{i,b} W_b)^2 + \dots \right]^{0.5} \quad [8]$$

where $W_{u,i}$ is the uncertainty value for principal component i , $V_{i,a}$ and $V_{i,b}$ are eigenvectors for solutes a and b for principal component i , and W_a and W_b are the analytical uncertainties. The uncertainty value for each component is then used to create two new sets (high estimate and low estimate) of values for $U1$ and $U2$. These new values of $U1$ and $U2$ are then used in Eq. [5–7] to calculate an uncertainty range for each event.

The chemistry of each end member was estimated as the median of samples taken before, during, and after an event. The temporal variability of the solute concentrations, particularly near stream groundwater and spring water, was small during the events. The short-duration, high-intensity rainstorms also had minimal temporal variability in rainwater chemistry, although concentrations changed during the 16-wk study period. The water chemistry in the saturated areas also did not change appreciably during the storm

events, but Si and DOC concentrations became diluted, and $\delta^{18}\text{O}$ values were enriched. Varying the tracer concentrations in the governing equations (Eq. [3], [5–7]) is recommended when temporal variability is large, although in this study more consistent results were found when the median concentrations were taken from all nine events. The assumption of static end members is unlikely across all events, but it provided an effective means for comparing a range of rainfall events.

Results

Mapping of Surface Saturation Patterns

Hillside and near-stream saturated areas were evident from simple field surveys. Six surveys were collected immediately before, during, and after the 2007 growing season (Fig. 2) using a hand-held GPS receiver. The saturation extent decreased after snowmelt through the summer (Fig. 2a–d); the estimate of saturation extent dropped from 9.90% after snowmelt to 1.70% of the surveyed area during the summer low flow. The location of saturation also shifted from near-stream areas after snowmelt to more fingerlike patterns originating from point sources. The consistent hillside saturation patterns were fixed by groundwater springs, which maintain downslope saturation through the driest periods.

The size of the saturated areas varied little during the dry summer conditions, changing from 1.7 to 4.3%, but responded rapidly to rainfall events. For example, the survey on 5 Sept. 2007 was made during summer low-flow conditions, before the rainfall events on 8, 9, and 11 Sept. 2007 (Fig. 2). The survey on 12 Sept. 2007 was made within 3 h of peak stream runoff from a 13-mm rainfall event. Comparing the 5 and 12 September surveys shows that the spatial extent of saturated areas increased more than twofold, as a result of 29 mm of rainfall across 3 d. The hillside saturated areas extended downslope and became temporarily connected to the stream in the 12 September survey. After the system wetted up during that event, the extent of saturated areas did not decrease appreciably again before the 5 Oct. 2007 survey, but the later survey lacked the overland connections to the stream (Fig. 2e, f). These simple surveys provided qualitative evidence of the spatial and temporal dynamics of overland flow paths and were used to validate the measurements made during the rainfall events.

Analysis of Nine Storm Events

Nine rain events were monitored across a 20-wk period from 4 July to 19 Oct. 2007. The rain events ranged from approximately 2.4 to 12.6 mm and occurred with a variety of antecedent rainfall conditions (Table 1). The average 15-min rainfall rate varied from 0.31 to 5.78 mm h^{-1} , and the rainfall events lasted from about 0.8 to 15.2 h. The maximum 15-min rainfall rate ($\sim 35 \text{ mm h}^{-1}$) did not exceed the estimate of saturated conductivity of 46 mm h^{-1} . The 7-d antecedent rainfall varied from approximately 0.0 to 8.7 mm, and the 21-d varied from about 0.5 to 28.1 mm.

The differences in rainfall and antecedent rainfall conditions produced a correspondingly large range of runoff conditions in the stream and hillside weirs. The length of the stream runoff events ranged from approximately 16 to 89 h and had average 3-d antecedent runoffs of about 0.05 to 0.23 mm d^{-1} (Table 2). The peak stream discharge varied from approximately 0.6 to 9.7 mm d^{-1} (Table 2) and lagged behind the rainfall by between 1.0 and 5.3 h. Overland flow occurred during every event at the SP1weir and the SPO weir, the same locations that maintained constant baseflow through the summer. The more transient SP2 and SP3 produced overland runoff in five of the nine events, presumably when small saturated areas formed above the weir. The mean discharge from the SPO was between 0.118 and 0.668 L s^{-1} , which was about ten times the discharge from SP1 during the nine events (Table 2).

Water-table heights were also measured at four locations along the hillslope: a riparian well, a near-stream transient piezometer, and two upslope piezometers. The water table responded to the nine rainfall events at all locations, but the rate of groundwater rise (starting at the beginning of rainfall and ending at maximum groundwater level) varied significantly between events from 4.7 to 55.9 cm h^{-1} for the PGW (Table 3). A water table (PGW) was maintained throughout the study period only at the riparian well, while the other piezometers measured a transient water table during rainfall events (NSGW, TGW1, TGW2) (Fig. 3). The transient response of a perched water table was caused by an impermeable fragipan layer at a depth of 30 to 70 cm (USDA 2007). The PGW responded more slowly and declined more gradually than the transient groundwater during the storm events (Table 3 and Fig. 3).

The hydrographs shown in Fig. 3 are indicative of the range of rainfall events measured and are used as examples in the following discussion. The events began with a small rainfall event with dry antecedent conditions on 8 Sept. 2007 (4 mm rainfall in previous 21 d), followed by larger events with wetter conditions on 11 September (13 mm rainfall in previous 21 d), and much wetter conditions on 19 October (20 mm rainfall in previous 21 d). During this time, the mean PGW height increased from 42 cm below the surface during the 8 September event to 14 cm during the 11 September event, and then to 11 cm during the 19 October event. Correspondingly, the runoff coefficients showed a large range: 0.14% during the 8 September event, which began with the driest antecedent conditions; 1.60% as the system wetted up during 11 September 7; and to 8.30% during the 19 October event, which had the most antecedent rainfall. The nine rainfall events thus represented a variety of conditions from which to assess common source areas and flow paths in the study watershed.

Groundwater Table–Stream Runoff Relationships

The groundwater table–stream runoff relationship showed significant variability depending on the antecedent conditions and

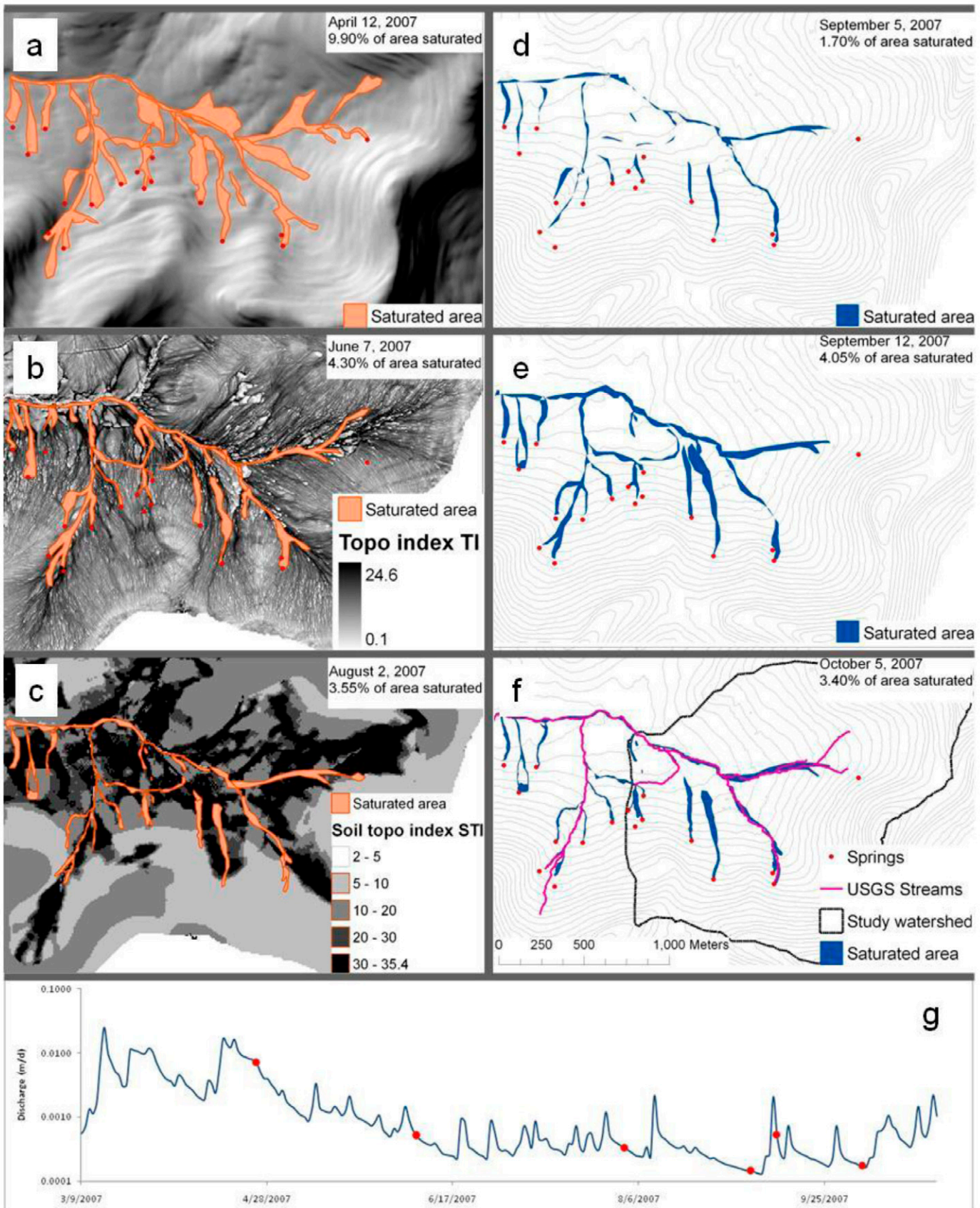


Fig. 2. Maps (a–f) of surface saturated areas constructed from six field surveys using the boot-print method of saturation and GPS system (to an accuracy of 3 m) Also included are (a) the hillshade (topography), (b) the topographic index, (c) the soil topographic index, (f) the USGS delineated stream discharge, and (g) discharge during the course of the study period. Red dots indicate times that surface saturation surveys were made.

Table 1. Rainfall information for nine storm events.

Measurement	Event date								
	7/4/07	7/23/07	9/8/07	9/9/07	9/11/07	9/27/07	10/9/07	10/10/07	10/19/07
Duration of rainfall (h)	1.33	0.83	3.80	10.50	14.50	15.20	10.17	5.50	7.83
Total rainfall (mm)	7.67	4.70	3.41	4.92	12.61	10.82	2.78	2.39	8.50
7-d antecedent rain (mm)	2.16	8.69	0.00	0.54	7.08	3.74	1.21	1.49	2.53
21-d antecedent rain (mm)	15.40	22.67	0.54	3.98	12.98	28.12	12.10	12.38	20.32
Maximum 15-min rainfall (mm h^{-1})	34.81	12.14	7.89	6.21	18.62	10.21	6.62	2.40	5.42
Average 15-min rainfall (mm h^{-1})	5.78	5.61	0.89	0.47	0.87	0.31	0.67	0.47	1.09

rainfall. The PGW heights showed a consistent counterclockwise hysteresis versus stream discharge (Fig. 4), indicating that the PGW lagged behind the stream response during the rising portion of the hydrograph (Fig. 3). The PGW lagged behind the stream response during both the 11 September and 10 October events, despite wetter antecedent conditions (Table 1) and a 20-cm difference in the prestorm PGW height during the 10 October event. The NSGW heights also had a counterclockwise hysteresis during the 11 September and 19 October events but peaked at the same time as the stream (Fig. 1). During both storms, the NSGW height began around 40 cm from the surface, rose rapidly, and then reached a maximum of about 10 cm, where it remained for 3 to 5 h. A 5- to 15-cm thick organic layer with highly conductive soils probably caused the water near the stream to move laterally at shallow depths and (effectively) to act as overland flow (Lyon et al., 2006b). Thus, while the NSGW heights remained close to 10 cm from the surface for much of the event, the upslope saturation areas were connected via overland flow, which was consistent with field observations during some of the larger events (Fig. 2b, e).

Overland Flow–Stream Runoff Relationships

The overland flow measurements at SP1 and the SPO had a small clockwise hysteresis, indicating that they responded faster than

the watershed outlet (Fig. 4c, d). The rapid response of the SP1 discharge resulted from a small saturated area below the spring head, whose size depended on the antecedent conditions (see Materials and Methods section). The SP1 discharge was more than 50% greater during the 11 September storm (Fig. 4d), despite wetter antecedent conditions during the 19 October event (Tables 1 and 2). These differences probably reflected the greater rainfall intensity during the 11 September event, which produced increasing amounts of saturation excess overland flow for the same saturated area (equivalent to infiltration excess Hortonian runoff from an area with negligible vertical hydraulic conductivity), versus a more constant rainfall intensity during the 19 October event (Fig. 3a, c). Conversely, the SPO response increased in a similar linear way during both events, supplying nearly twice as much runoff in the 19 October event as in the 11 September event (Fig. 4c). The sources feeding the soil pipe were not clear because there were no distinguishable upslope saturated areas and the nearby TGW1 response lagged.

Tracer Response

The rainfall caused consistent deflection in $\delta^{18}\text{O}$ values in the stream water during the storm events (Fig. 5). The $\delta^{18}\text{O}$ response reflected the addition of isotopically enriched event water during

Table 3. Groundwater level information from nine storm events for permanent groundwater (PGW), near-stream groundwater (NSGW), transient groundwater, valley bottom (TGW1), and transient groundwater, hillside (TGW2).

Measurement†	Event date								
	7/4/07	7/23/07	9/8/07	9/9/07	9/11/07	9/27/07	10/9/07	10/10/07	10/19/07
Mean PGW height	44.9(4.7)‡	32.1 (55.9)	41.9 (6.1)	34.3 (7.5)	13.9 (26.6)	16.4 (34.6)	20.3 (15.4)	11.7 (6.2)	10.7 (12.3)
Maximum PGW height	43.8	9.4	38.9	32.5	7.1	7.3	15.3	10.3	7.7
Mean NSGW level	41 (7.4)	31.6 (38.6)	35.9 (6.4)	36.7 (9.2)	23 (47.8)	22.8 (20.5)	24.6 (17.6)	22.1 (6.4)	20.8 (25.8)
Max NSGW level	37.9	19.9	30.6	30.6	7.8	13.4	20.6	18.2	7.9
Mean TGW1 level	23.7 (41.7)	18.6 (21.8)	42.6 (1.4)	43.9 (0.3)	22.2 (57.4)	29.7 (17.4)	55 (0.5)	43 (31)	19.9 (53.1)
Max TGW1 level	8.5	9.6	42.4	43.8	0.9	17.9	54.7	36.3	4.0
Mean TGW2 level	38.9 (2.6)	39.8 (1.7)	36.8 (3.1)	37.3 (0)	22.2 (41.4)	42.3 (12.5)	25.1 (9.5)	19.3 (15.4)	19.6 (28.6)
Max TGW2 level	38.0	39.1	35.0	37.2	2.2	35.1	20.2	12.7	1.0

† Distance from surface (cm).

‡ Numbers in parentheses are rise rates (cm h^{-1}) for groundwater increase at the initiation of rainfall.

Table 2. Runoff information for nine storm events. Runoff event information is given for the stream and for four weir locations.

	Event date								
	7/4/07	7/23/07	9/8/07	9/9/07	9/11/07	9/27/07	10/9/07	10/10/07	10/19/07
Length of stream runoff event (h)	46.8	33.4	16.2	26.8	89.3	36.1	21.8	28.8	76.3
3-d antecedent average stream runoff (mm d^{-1})	0.050	0.118	0.046	0.052	0.065	0.073	0.132	0.147	0.227
Stream runoff volume (mm)	0.038	0.075	0.051	0.116	0.479	0.345	0.063	0.134	0.706
Stream discharge, time to peak (h)	1.5	2.2	5.3	1.8	1.0	2.5	2.5	2.3	1.3
Peak stream discharge (mm d^{-1})	2.15	0.63	0.90	1.49	4.66	3.65	2.41	2.46	9.69
Mean soil pipe outlet discharge (L s^{-1})	0.143 (0.012)†	0.206 (0.043)	0.118 (0.005)	0.125 (0.004)	0.143 (0.045)	0.668 (0.171)	0.534 (0.028)	0.582 (0.022)	0.279 (0.094)
Mean spring 1 discharge (L s^{-1})	0.161 (0.007)	0.159 (0.004)	0.053 (0.008)	0.051 (0.007)	0.067 (0.017)	0.074 (0.017)	0.069 (0.003)	0.073 (0.005)	0.076 (0.007)
Mean spring 2 discharge (L s^{-1})	0	0	0	0	0.022 (0.017)	0.041 (0.003)	0.043 (0.004)	0	0.066 (0.002)
Mean spring 3 discharge (L s^{-1})	0	0	0	0	0.019 (0.033)	0.114 (0.03)	0.012 (0.007)	0	0.018 (0.033)

† Numbers in parentheses denote standard deviations.

the rainfall events. The mean rain $\delta^{18}\text{O}$ value was $-4.92 \pm 0.87\text{\textperthousand}$ during the nine events (Table 4) compared with an average stream baseflow value of $-10.61 \pm 0.57\text{\textperthousand}$. The baseflow (pre-event) $\delta^{18}\text{O}$ was a mixture of enriched near-stream groundwater (mean = $-9.73\text{\textperthousand}$) and depleted groundwater springs (mean = $-10.91\text{\textperthousand}$) that discharged directly into the stream from zero-order tributaries (see spring location in Fig. 2). The $\delta^{18}\text{O}$ values of the stream ranged from -10.85 to $-8.55\text{\textperthousand}$ and were positively correlated to stream discharge ($r^2 = 0.69$) during the nine events.

The Si concentration of the stream decreased during the rainfall events ($r^2 = 0.50$), and DOC concentrations increased more linearly ($r^2 = 0.72$) (Fig. 5). The variability in the Si concentration was relatively small during the events, 1.32 to 2.0 mg L^{-1} , with minimums during peak flows consistent with dilution-type effects (rain Si concentrations are 0.06 mg L^{-1} , Table 4). Conversely, DOC concentrations reached their maximum at peak discharge (indicating flushing effects) and had more variability,

baseflow concentrations were around 5 mg L^{-1} , and peak flow concentrations were between 10 and 20 mg L^{-1} . The timing of the tracer response was also different because Si and DOC

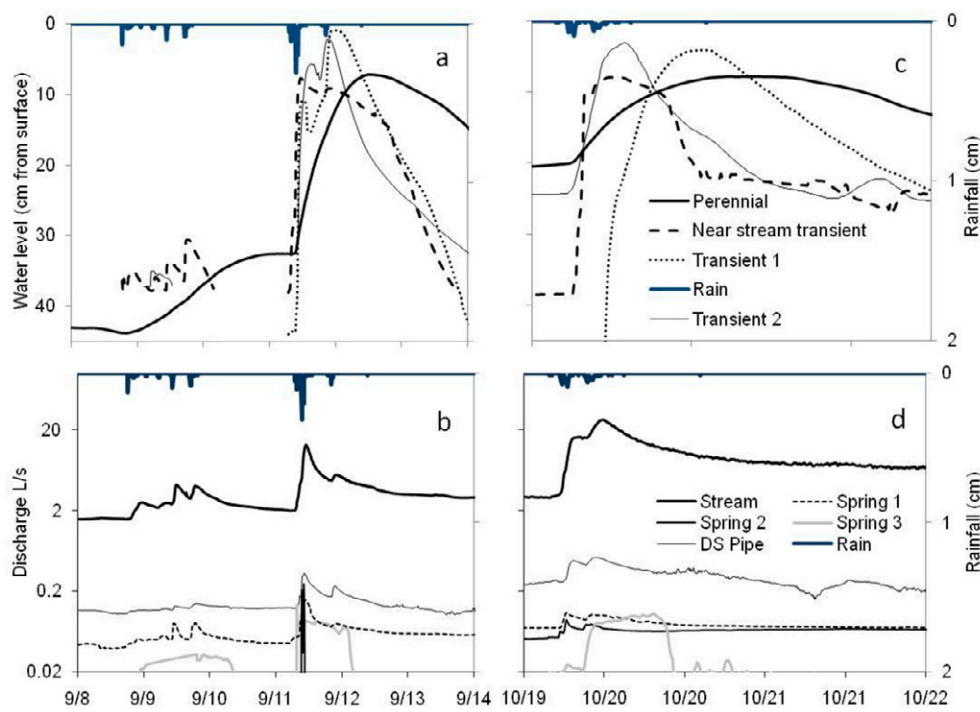


Fig. 3. Temporal water table (a, c) and discharge response (b, d) for 8, 9, and 11 Sept. 2007 and 19 Oct. 2007, respectively. Transient groundwater was not measured for most of 8–9 September and at other points when not shown. Discharge response is shown on a log axis to compare all overland flow measurements. Data not shown indicates that the water table fell below the bottom of the piezometer (i.e., in [a], transient groundwater 1 and 2 on 8 September) or discharge was zero (e.g., in [a], DS pipe and spring 3 on 8 September).

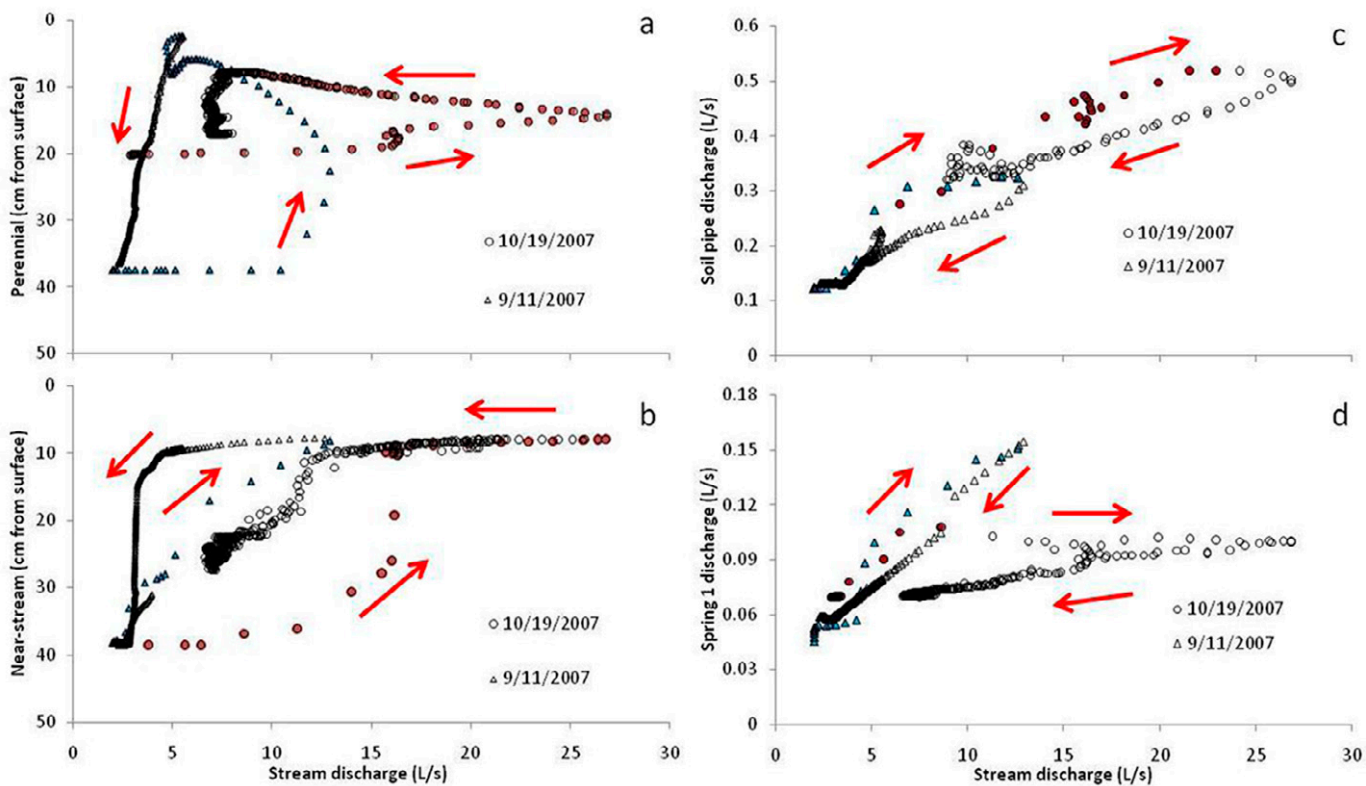


Fig. 4. Temporal relationships during the 11 Sept. and 19 Oct. 2007 events between the stream and (a) PGW, (b) NSGW, (c) SPO, and (d) SP1. Comparisons are made every 15 min and arrows indicate direction of hysteresis. Filled symbols represent measurements made during the rising portion of the hydrograph.

concentrations and $\delta^{18}\text{O}$ values responded rapidly to increasing discharge, but DOC fell immediately, while Si and $\delta^{18}\text{O}$ remained depleted for up to 24 h after the event (Fig. 5). The magnitude and timing of the concentrations in the stream reflected additional runoff sources during the rainfall events.

Solute concentrations were also measured at different end members across the hillslope during the nine events (Fig. 1 and Table 4). As mentioned previously, the rain and throughfall were enriched in $\delta^{18}\text{O}$ and had much lower concentrations of DOC and Si than the stream water. The PGW and SP1 water showed the opposite chemistry, being more depleted in $\delta^{18}\text{O}$ and having higher concentrations of Si. The DOC concentrations varied significantly across the landscape, from less than 3 mg L^{-1} in spring waters to about 8 mg L^{-1} in the riparian groundwater and soil water and to much a higher concentration (25.0 mg L^{-1}) in the near-stream saturated areas. The tracer concentrations and isotopic ratios were used subsequently to estimate the source areas of runoff with simple hydrograph separation techniques.

Event-Water Response

A simple two-component mixing model (Eq. [3]) was used to separate streamflow into event-water (event rainwater) and pre-event-water (baseflow water) contributions during nine storms. The

contribution of event water was 14 to 37% of the runoff volume, with the maximum storm contribution from 18 to 49%, usually near peak stream discharge (Table 5 and Fig. 6a, c). The proportion of event-water contributions was clearly a function of rainfall characteristics and antecedent conditions. For example, during three successively larger storms in September (Fig. 3), the event-water contributions increased from 13.6 to 25.0 and then to 36.9% as the system wetted up (Table 5). The timing of the event water also became less delayed and more synchronized with the stream discharge during the 11 September storm. However, during the 19 October storm, which had very wet antecedent conditions, event water composed only 33.1% of the total volume (Table 5), because groundwater contributions were larger due to greater baseflow (Fig. 6). Overall, the event-water contributions during these nine storms were strongly correlated to the rainfall volume (the Pearson product-moment correlation coefficient, reported as r values, was $r = 0.69$), but less so by the 7-d or 21-d antecedent rainfall ($r = 0.20$ and 0.41 , respectively).

The event water reached a consistent maximum of around 35% during the three largest events (11 and 12 Sept. and 19 Oct. 2007) despite varying rainfall intensities and antecedent conditions. Across all of the events, the maximum event-water contributions were correlated more to the length of the rainfall event and volume ($r = 0.70$ and 0.79 , respectively) than to the mean or maximum

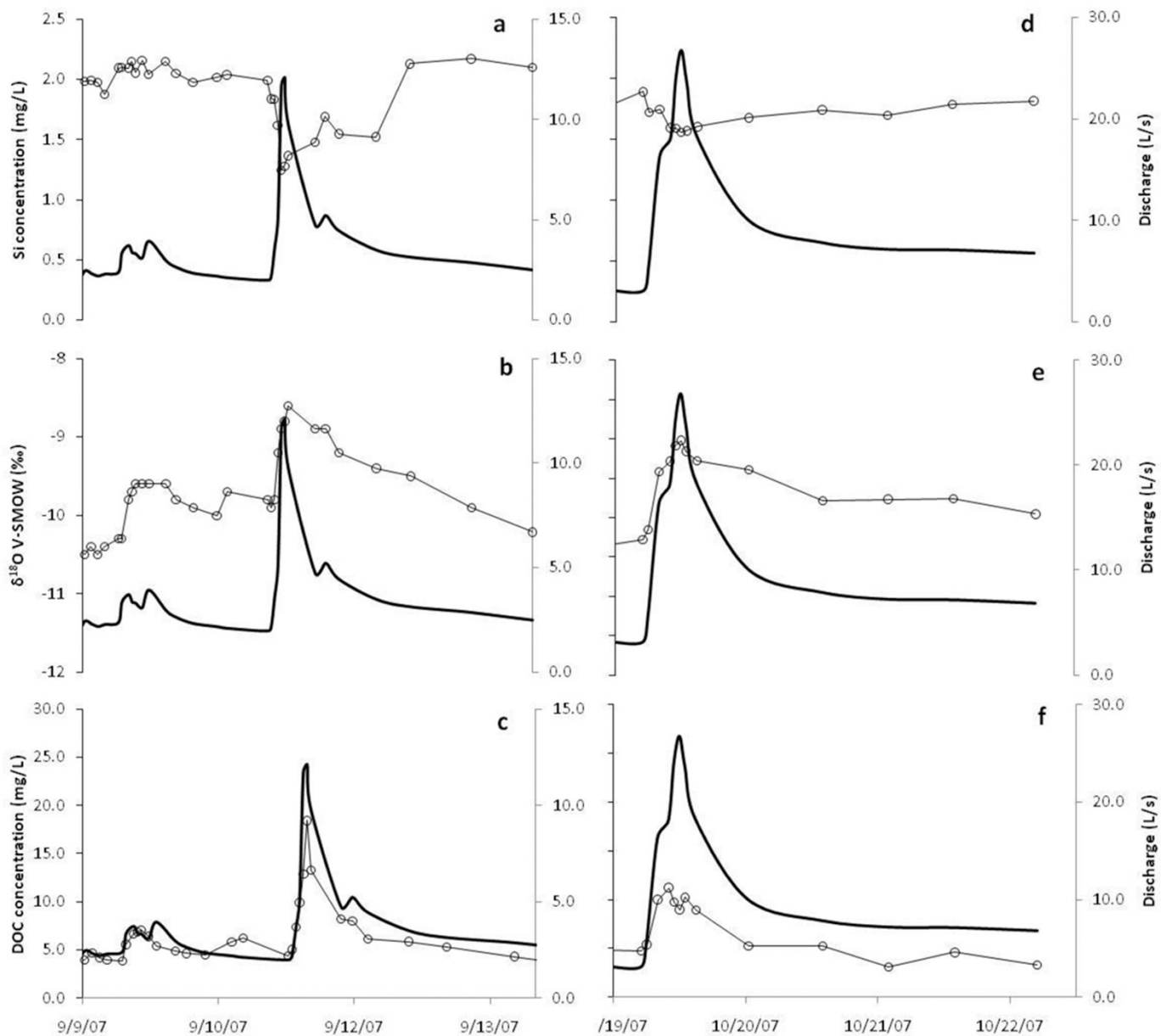


Fig. 5. Chemographs (connected circles) and hydrographs (solid lines) for 8, 9, and 11 Sept. 2007 storms: (a) Si concentration, (b) $\delta^{18}\text{O}$, and (c) DOC; and for 19 Oct. 2007 storm: (d) Si concentration, (e) $\delta^{18}\text{O}$, and (f) DOC. The Si concentrations and $\delta^{18}\text{O}$ values show consistent dilution during storm events versus a flushing of DOC concentrations.

15-min rainfall intensity ($r = 0.61$ and -0.24 , respectively). The error estimated with Eq. [8] is shown for each stream sample in Fig. 6a, and c, with errors from 12.4 to 30.1% of the storm volume for the nine events. Overall, the two-component model demonstrated that event rainwater is an important source of runoff during summer storms.

End-Member Response

The responses of the three solutes, Si, DOC, and $\delta^{18}\text{O}$, were used to identify water source areas using EMMA and Eq. [5–7]. Viable end members were selected using the concentration plots between

the various solutes (Fig. 6). A groundwater end member was necessary to explain the high Si concentrations and depleted $\delta^{18}\text{O}$ values during the entire event (Fig. 7), particularly during baseflow. The more enriched $\delta^{18}\text{O}$ values and lower Si concentrations were attributable to rain and throughfall sources (Fig. 7). The depleted rainfall $\delta^{18}\text{O}$ values did not change by more than 1.5‰ during any of the short rainfall events, with a mean of $-4.92\text{\textperthousand}$ and standard deviation of 0.87‰ for all nine events (Table 4). Neither the soil water from the A-horizon nor the shallow groundwater could explain the DOC concentrations in the stream (Fig. 7). Instead, saturated areas were the only source capable of producing high stream DOC concentrations (Fig. 7), which exceeded 15 mg L^{-1} at peak storm

Table 4. Solute concentrations and isotopic values for the end-members used in the mixing analysis. The end-members are averaged from multiple measurements during all nine storm events.

Measurement	End member		
	Si mg L ⁻¹	$\delta^{18}\text{O}$ ‰	DOC mg L ⁻¹
Mean rain and throughfall	0.06 (0.04)†	-4.92 (0.87)	1.03 (0.43)
Mean perennial near-stream groundwater	1.68 (0.15)	-9.73 (0.26)	7.68 (1.56)
Mean spring groundwater	1.9 (0.11)	-10.91 (0.25)	2.49 (1.03)
Mean saturated area	0.69 (0.16)	-8.84 (0.48)	24.97 (3.05)
Mean soil water	0.92 (0.59)	-6.04 (1.87)	7.06 (1.15)

† Numbers in parentheses indicate standard deviations.

flows (Fig. 5). Soil water was excluded from the EMMA because its $\delta^{18}\text{O}$ values were not distinguishable from those of rainwater, and the volume of water collected from the free-draining lysimeters was minimal and erratic, producing runoff in only four of nine events. Thus, the concentration plots suggest that a three end-member system is necessary to explain stream response: groundwater (baseflow water), saturated areas, and rain water.

Principal component analysis was used to define a mixing space for the nine events using the three end members for each event. This model explains 90 to 98% of the variability (depending on the storm) in Si and DOC concentrations and $\delta^{18}\text{O}$ values for the nine storm events, implying that three end members are beneficial (Fig.

8). The first principal component was controlled by the dilution of Si and $\delta^{18}\text{O}$, while the second was controlled by the flushing of DOC. The percent contributions for the three end members during the nine storm events are shown in Table 5. The groundwater dominated the volume of stream water during storm events, producing 53 to 95% of total runoff volume (Table 5). The volume of rainwater ranged from 4 to 25%, and saturated areas were between 2 and 24% of the total storm volume for the nine storm events (Table 5). The model was adequate in reproducing the measured values, with r^2 values ranging from 0.55 to 0.77 for Si, 0.76 to 0.97 for DOC, and 0.85 to 0.99 for $\delta^{18}\text{O}$. The error estimates made using Eq. [8] are shown for select rain events in Fig. 6b and d for all three end members and varied from 8 to 31% of the total storm volume during the nine events.

Contributions from saturated areas reached their maximum during peak stream discharge and then fell rapidly, while the contributions from rainwater were more damped and lagged behind the runoff peak (Fig. 6). During the 11 September storm event, maximum saturated area contributions exceeded 59% of peak streamflow compared with a maximum of 22% from rainwater, which came after peak streamflow. This same trend is also evident from the PCA plot (Fig. 8), which showed a rapid expression of saturated areas in the stream water followed by rainwater during the falling portion of the hydrograph for both the 11 September and 19 October storm events. Combining the saturated-area and rainwater contributions gave a runoff volume with similar timing and magnitude to the event water estimated with the two-component model (Eq. [3]) for both events in Fig. 6a, c. The relative agreement between the two models suggests that the EMMA results are a plausible explanation for sources of event water.

Table 5. Results from mixing models and hydrograph separations for nine storm events.

Parameter	Event date								
	7/4/07	7/23/07	9/8/07	9/9/07	9/11/07	9/27/07	10/9/07	10/10/07	10/19/07
% ——————									
2-component model									
Runoff coefficient	0.49	1.39	0.14	1.39	1.60	3.07	2.24	5.59	8.30
Saturated area†	N/A	N/A	1.3	1.3	3.1	N/A	2.3	N/A	N/A
Volume new water	14.9	15.2	13.6	25.0	36.9	36.4	21.7	26.6	33.1
Maximum proportion new water	22.5	23.2	17.5	28.1	45.6	49.0	26.6	28.0	49.2
3-component model									
Volume rain and throughfall	15.8	7.0	3.6	6.5	14.5	18.9	11.3	13.1	24.8
Volume saturated areas†	11.2	20.7	1.5	5.8	28.4	24.2	15.8	21.5	22.5
Volume groundwater	73.1	72.3	95.0	87.7	57.1	56.8	72.9	65.5	52.8
Maximum proportion rain and throughfall	21.5	16.9	5.8	10.1	22.2	29.3	16.7	15.6	31.6
Maximum proportion saturated areas†	17.7	32.3	3.9	10.3	59.3	49.6	23.9	30.1	33.9

† Saturated areas are estimated for selected events via field surveys (see Fig. 2).

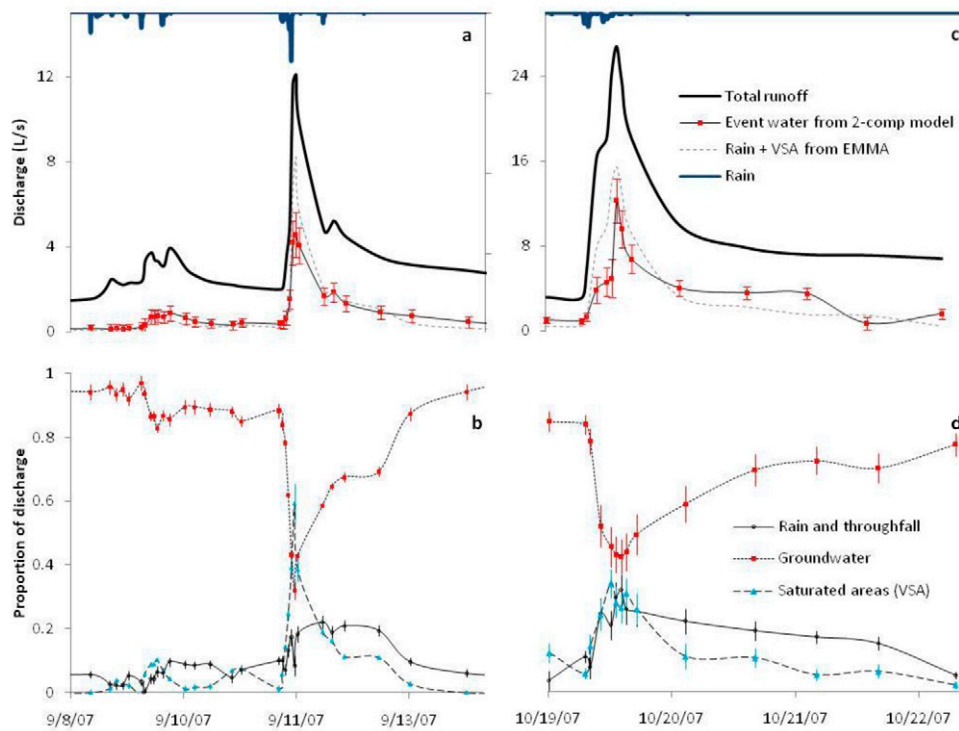


Fig. 6. Hydrograph separations using simple mixing models for (a, b) 8, 9, and 11 Sept. 2007 storms and (c, d) 19 Oct. 2007 storm. Top graphs show separation of new event water using the two-component model and rain plus saturated areas from three-component model. The bottom graphs show the contributions of the three-component model using Si, DOC, and $\delta^{18}\text{O}$.

Discussion

Saturation excess runoff is an important contributor to storm response in the northeastern United States but remains difficult to quantify spatially and temporally because of the lateral redistribution of water. In the Town Brook watershed, lateral preferential flow paths could potentially connect hillside areas to the stream, making predictions difficult with conventional VSA models. In another example from the hillslope used in our study, Lyon et al. (2006b) showed that the topographic index was insufficient to predict the likelihood of surface saturation during drier summer conditions.

Causes of Soil Saturation in Town Brook

The spatiotemporal patterns of surface saturation were different between valley-bottom areas and hillside areas far from stream channels (Fig. 2f). After snowmelt on 12 Apr. 2007, saturated areas adjacent to the stream channel (within 15 m) represented about 80% of the total extent of surface saturation (Fig. 2a). The near-stream saturation areas accounted for only 55% of the saturation area during the driest survey, on 5 Sept. 2007, with the remaining soil saturation occurring in isolated areas on the hillsides that were not connected to the stream (Fig. 2d). Hillside saturation areas maintained by groundwater springs have been described throughout the Catskills (Burns et al., 1998; West et al., 2004; Soren, 1963). The differing controls on saturation areas in the

valley bottoms versus the hillsides may inhibit the applicability of conventional VSA prediction techniques.

Qualitative comparisons of the saturation areas estimated using surface topography and soil properties with the measured saturation areas suggest that additional information may be required for robust prediction of VSA patterns at this site. The TI calculated using a 5- by 5-m DEM (Fig. 2b) correctly identified most hillside saturation areas, but even high-resolution light-detection-and-ranging topography cannot reproduce the concentrated overland flow from the spring heads. Additionally, the TI would have predicted that the valley-bottom areas should remain saturated during drier conditions because of larger contributing areas than the upslope areas; however, the continuous spring discharge maintained hillside saturation areas, while the valley-bottom contributions decreased quickly after snowmelt (Fig. 2a, b). The STI even more severely overpredicted valley-

bottom saturation because the Onatea soils (Fig. 1 and 2c) have lower hydraulic conductivity. This qualitative analysis showed that TI and STI generally overpredicted the extent of near-stream saturation areas and underestimated the importance of upslope lateral preferential flow paths.

Previous studies in Town Brook have also shown that measured saturation areas are generally overpredicted by VSA models that are based on surface topography and soils information. Working in an adjacent north-facing Town Brook tributary approximately 2 km west of the watershed in our study, Mehta et al. (2004) showed that hillside saturation areas were concentrated and connected to the stream but were poorly predicted by their distributed model (see Mehta et al., 2004, Fig. 10). Even with inclusion of microtopography, the model severely overpredicted the extent of saturated areas near the stream channels and did not capture small hillside areas caused by groundwater springs (see Mehta et al., 2004, Fig. 12). Additionally, Lyon et al. (2006a,b) used 43 piezometers in a 120- by 180-m area at the toe of the study hillslope (Fig. 1) to estimate the shallow groundwater table. They found that the STI had a relationship to the probability of surface saturation during wet conditions (March to May) but not during dry conditions (June to August). A reanalysis of toe-slope saturation patterns from Lyon et al. (2006b) shows that during dry conditions (see Lyon et al., 2006b, Fig. 5) the most persistent saturation occurred at the SPO

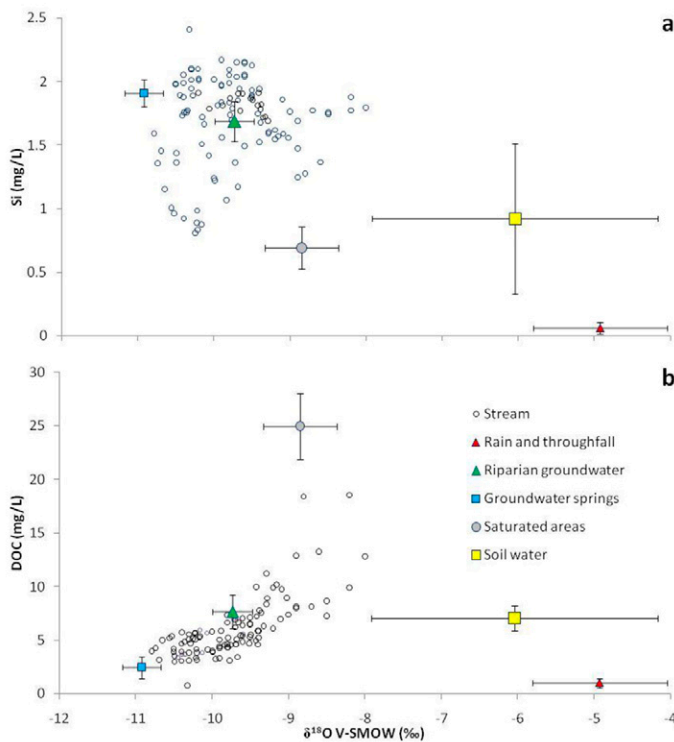


Fig. 7. Solute concentrations and isotopic values for all nine storm events and average end-member concentrations and values. Groundwater (spring and riparian waters) capture most of the stream concentrations, but a DOC-rich source and enriched $\delta^{18}\text{O}$ source are necessary to capture all the variability.

in the northwest corner of the hillslope (Fig. 1 and 2). We would expect that runoff from these localized saturation areas may be less important during wet conditions, but runoff events were not measured during wetter spring conditions (Fig. 2). The lack of agreement between predictions and measurements of saturation areas during drier conditions in Town Brook appears driven by lateral preferential flow paths, such as the springs and soil pipes, that are not well described by the surface topography and soil surveys.

The role of lateral preferential flow paths is better examined in regard to the hillslope geomorphology and geology. The contact groundwater springs result from bedding planes in the sandstone bedrock (Reynolds, 2000) but are not predictable by elevation or upslope area. Instead, the hillside saturation areas consistently emerge at the interface between the Willowmoc and Lackawanna soils (Fig. 1), where the vertical hydraulic conductivity decreases (see STI in Fig. 2c) and the fragipan becomes more consistent. The hillside saturation areas rarely extend to the near-stream Onteora soils (Fig. 2c) because the Willowmoc soils on the toe slope (Fig. 1) have reduced slopes and increased soil depths. On the study hillside, the Willowmoc soils also contain at least two measured soil pipes at depths of less than 0.75 m that extend to within 300 m of the stream. The soil pipes occur within the Willowmoc soils but discharge into the flat, poorly draining Onteora soils and create one of the few consistent near-stream saturation areas (Fig. 2; see

also Lyon et al., 2006a). The near-stream saturation areas are influenced by the upslope lateral preferential flow paths, but their relative influence on watershed functioning remains unexplored. In general, the lateral preferential flow paths at Town Brook are linked to increased rapid surface and shallow subsurface runoff and reduced vertical infiltration (or changes the runoff typology).

Importance of Lateral Preferential Flow Paths to Storm Runoff Sources

Evaluating the impacts of lateral preferential flow paths on watershed functioning requires inferences from the hydrometric, chemical, and isotope data because direct, robust measurements are impractical. In Town Brook, preferential flow occurs both during low flows and transiently during rainfall events due to a variety of causes, including bedrock heterogeneities, overland flow paths, microtopography, and soil piping. The lateral preferential flow paths accentuate lateral runoff and may reduce the role of topography and topology (i.e., channel drainage network) on runoff source areas if they connect to the stream.

Several hydrometric lines of evidence suggest that hillside saturation areas connect to the stream channel during rain events. First, GPS measurements made after snowmelt (Fig. 2a) and within 3 h of the 11 September rain event (Fig. 2f) showed saturated connections from the spring head down to the stream channel. Second, the overland flow measurements at the springs and soil pipe responded faster to rainfall events than the stream did (Fig. 4c, d), implying they could be a source of peak storm runoff. Third, the transient NSGW also responded rapidly and remained within 10 cm of the surface, where the lateral conductivity in the organic horizon is much higher than in the mineral soil (Fig. 4b). This type of transmissivity feedback type response has been found in other studies in till soils (Bishop et al., 1990; Kendall et al., 1999) and is indicative of fast-runoff flow paths and high DOC concentrations (Kendall et al., 1999). In this study, the shallow flow in the top 5–10 cm was essentially overland because the vertical infiltration was near zero and these areas appeared saturated using the boot-print survey method shown in Fig. 2. Finally, the deeper PGW and nearby TGW1 did not respond fast enough to contribute to the peak stream discharge (Fig. 3a, c and 4a), with the most extreme case being the unexplained 8-h lag of TGW1 during the 19 October event. The entirety of the hydrometric observations suggest that surface saturation in near-stream areas stayed connected to the stream during rain events and acted as a flow path that connected the hillsides to the stream.

The water chemistry was also used to estimate source areas via simple hydrograph separations. The simplest two-component model using $\delta^{18}\text{O}$ values convincingly showed that water supplied by the rain event (event water) was a significant source of runoff, especially during peak streamflow (Fig. 6 and Table 5). This result implied that source areas and flow paths combined to rapidly contribute event water to the stream during the rising portion of the

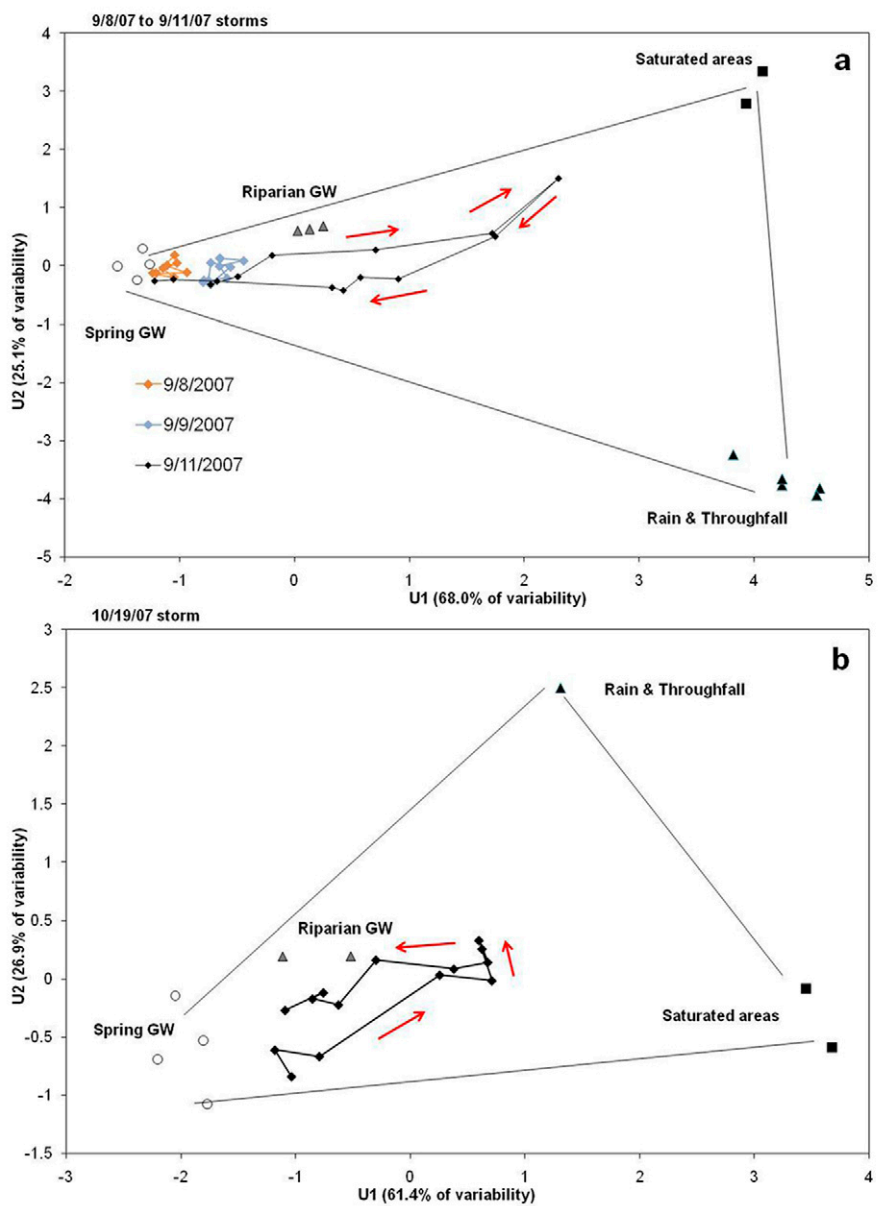


Fig. 8. Principal component analysis used in the three-component mixing model for (a) 8, 9, and 11 Sept. 2007 storms and (b) 19 Oct. 2007 storm. The first principal component is mainly explained by Si concentrations and $\delta^{18}\text{O}$ values, while the second is mostly explained by the DOC concentrations.

hydrograph. However, EMMA using several tracers ($\delta^{18}\text{O}$, Si, and DOC) showed that stream contributions from rainwater lagged behind and were damped compared with the stream response (Fig. 6b, d). The rapid contributions during the rising portion were instead supplied by saturated areas, which supply up to 24% of the runoff volume and 18 to 49% at peak streamflow. Combining the saturated-area and rain contributions from EMMA produced a hydrograph similar to that of the event water estimated using the two-component model (Fig. 6a, c), but the event water discharge was slightly smaller (<10%) during peak streamflow. These results imply that event water was mobilized both by direct precipitation

onto the stream channel and also from water that mixed in the saturated areas during peak flows. The EMMA relied on DOC to act as conservative tracer for saturated areas to be accurately predicted (Fig. 5).

The large flush of DOC during the rising limb of the hydrograph could only be explained by concentrations in the near-stream saturated areas (Fig. 7a). Other studies have found that the variability of DOC concentrations in streamwater may be an effective indicator of flow paths during storm runoff (Moore, 1989; McDowell and Fisher, 1976; Fiebig et al., 1990; Brown et al., 1999). Fiebig et al. (1990) suggested that DOC indicated flushing from preferential flow paths that were further from the stream channel and did not contribute during baseflow. The consistent trend of higher DOC concentrations on the rising versus the falling portion of the hydrograph (Fig. 5) was similar to trends in Maimai, New Zealand (Moore 1989), and in a small hardwood watershed in Massachusetts (McDowell and Fisher, 1976). Brown et al. (1999) also found that shallow soils were the most important source of DOC and a possible source of quick runoff in the Catskill Mountains. The EMMA suggested that the DOC is rapidly mobilized through shallow layers or preferential flow paths or both, while rainwater that was diluted in DOC dominates after peak streamflow.

Contributions from rainwater (event water that does not mix in the saturated areas) reached their maximum of 5.8 to 31.6% of the instantaneous discharge during the falling portion of the hydrograph (Fig. 6b, d). Similar dilution effects have been attributed to direct precipitation onto riparian saturated areas (Eshleman et al., 1993; Wels

et al., 1991). However, Buttle and Peters (1997) found that hillslopes were capable of generating event runoff from preferential flow paths that was often attributed to direct precipitation onto saturated areas. Buttle and Peters (1997) also suggested preferential flow paths could invalidate some common assumptions in hydrograph separation techniques unless the hydrometric response is taken into consideration. The results presented here agree with those of Buttle and Peters (1997) that lateral preferential flow paths are capable of transporting rainwater long distances to the stream channel without considerable mixing. If the intensive hydrometric measurements had not been collected, this rainwater contribution

could have erroneously been attributed to direct precipitation onto near-stream saturated areas (e.g., Wels et al., 1991). However, the results presented here cannot preclude additional contributions of rain (event) water via subsurface preferential flow paths occurring from a transient perched water table.

Separately the hydrometric and water chemistry results suggest that water supplied to saturated areas during peak storm runoff may originate from hillside sources, but an integration of these data sets could further corroborate this runoff mechanism. The rainfall events shown in Fig. 3a and b during several September rain events further illustrate hillside contributions. The 5 September survey (Fig. 2d) was made during summer low flow, and the total saturated area in the study watershed was 1.1%, but 0.21% was connected to the stream via surface saturation (essentially only the stream channel). Correspondingly, the rainfall event on 8 September had a very small runoff coefficient (0.14%), and the runoff was probably generated principally from direct precipitation onto the stream channel and not from saturated areas (3.6 versus 1.5% of the total runoff volume, respectively). As a result of this storm event, the water-table heights increased (Table 3 and Fig. 3b), and although no measurements were made at this time, the saturation extents probably increased. The subsequent 9 September storm had roughly equal contributions from rain and saturation areas (6.5 versus 5.8% of the total runoff volume, respectively), but saturation contributions could still be explained by a small near-stream area (<0.10% of the watershed area). However, during the larger event on 11 September, when the hillside saturation areas were connected to the stream, the volume contributed by saturation areas increased to 28.4% of the total and to 59.3% at peak streamflow. The near-stream saturation areas are not of sufficient size to generate this volume of runoff, which suggests that water from the hillside areas was quickly transported to the stream via lateral preferential flow paths under these conditions. The changing saturation areas during these September storms are an example of how antecedent conditions and rainfall characteristics act to influence runoff sources in Town Brook.

Conceptualizing Runoff Source Areas during Varying Growing-Season Storms

The antecedent conditions and rainfall characteristics unevenly controlled the hydrometric response between differing parts of the watershed. The rate of groundwater rise after the initiation of rainfall is used as a surrogate for soil water storage because of the difficulty in estimating drainable porosity in areas with lateral preferential flow paths and a lack of distributed soil moisture measurements at the hillslope. The rate of groundwater rise at the NSGW and PGW was strongly correlated to the 7-d antecedent rainfall conditions ($r = 0.89$ and 0.90 , respectively). In contrast, the upslope transient groundwater (TGW1 and TGW2) was more strongly explained by the total amount of rainfall ($r = 0.65$ and 0.65) than by the 7-d antecedent rainfall ($r = 0.45$ and 0.35). The same was true for overland flow at SPO, SP1, SP2, and SP3, where

the increase in discharge was more correlated to the storm rainfall volumes ($r = 0.60$, 0.57 , 0.77 , and 0.78 , respectively) than to the 7-d antecedent rainfall ($r = 0.29$, 0.26 , 0.54 , and 0.23 , respectively). The difference in response probably reflected the redistribution of water to near-stream areas, while the hillside features had a more limited “memory” of past rain events.

The differences in hydrometric response across antecedent conditions manifested in the differing runoff sources to the stream during the storm events. The volume and maximum instantaneous event-water contributions were much more correlated with rainfall volume ($r = 0.69$ and 0.79 , respectively) than with the 7-d antecedent rainfall ($r = 0.20$ and 0.30 , respectively). The rainfall contributions from EMMA also showed more correlation with total rainfall volumes ($r = 0.60$) than 7-d antecedent rainfall ($r = 0.10$). However, the total and maximum contributions from the saturated areas showed similar positive correlation to rainfall amounts ($r = 0.57$ and 0.68 , respectively) and 7-d antecedent rainfall ($r = 0.68$ and 0.63 , respectively). As a result of these antecedent and storm-related factors, the three rainfall events larger than 8 mm produced a similar volume of runoff from the saturated areas (22.5 to 28.4% of the total), while rain water contributions were more variable (14.5 to 25.8%) and increased more linearly with rainfall volume.

From a synthesis of these results, we propose a conceptual model capable of predicting the source areas for different combinations of antecedent conditions and rainfall characteristics. During smaller rainfall events and drier conditions, the hillside saturation areas remain disconnected, near-stream saturation areas are minimal, and most storm runoff is generated by direct precipitation onto the stream channel. A similar storm would generate more saturation excess overland flow in wetter antecedent conditions, when the PGW and NSGW respond more quickly. For storms with more than 8 mm of total rainfall, the additional sources and timing of overland flow can only be explained by the connection of hillside saturation areas to the stream. However, the hillside saturation areas have a maximum spatial extent that they quickly reach in wet antecedent conditions because of the limited upslope expansion of the lateral preferential flow paths (results shown in Fig. 2e, f and measurements from SP1 corroborate this). Larger rainstorms thus produced a similar amount of runoff volume from saturated areas but larger relative amounts of rainwater. The lagged contribution of the rain- and event water (Fig. 6) implies that direct precipitation onto the stream channel was not the only source of rainwater to the stream; instead, preferential flow paths could move rainwater from the hillsides, and the water's travel time to the stream could explain the lagged response in stream chemistry. This conceptual framework reinforces the idea that isolated areas in the landscape can contribute the majority of storm runoff through saturation excess processes under drier growing-season conditions.

Implications for Modeling and Management of VSA Hydrology

These results add to the growing body of evidence that highly responsive soils on the hill sides can be important contributors to storm runoff in co-evolved glacial soils (Buttle, 2006; Soulsby et al., 2006; Soulsby and Tetzlaff, 2008). It is clear that predicting the exact positions of saturated contributing areas may not be possible because of heterogeneities in the geology and soils. We believe that these heterogeneities are responsible for the surface saturation patterns observed in Town Brook and that they deliver the major source of storm runoff during larger summer and fall rainfall events. Although the stream chemistry would suggest a more shallow soil source, the mixing of overland flow and subsurface waters in near-stream areas means that alternative processes cannot be excluded as possible sources. What is apparent is that runoff sources and flow paths rapidly deliver water that has been mixed in the saturated soils and slowly supply event (rain) water during the stream recession.

A qualitative assessment of conventional VSA models at the Town Brook watershed suggested that they would be adequate for some management decisions but that they generally failed to capture the isolated flow paths on the hillsides and overpredicted the near-stream saturation extents (Fig. 2b, c). The inadequacies of VSA models in predicting these hillside runoff sources probably stem from a combination of two failings in such models: (i) a lack of spatial resolution in the input data that could parameterize these fine-scale lateral flow paths, and (ii) inadequate incorporation of lateral preferential flow paths into the model structure. The shortcomings in the structures and parameterization of the VSA models result in lateral conductivity estimates that are much larger than those given by soil survey information (e.g., Mehta et al., 2004) and reduce the influence of channel network topology on runoff sources. In other areas with coevolved glacial soils, hydrologic soil classification schemes have been developed (e.g., HOST classifications from Scotland, <http://www.macaulay.ac.uk/host/>, accessed 19 Apr. 2010) to better predict landscape-scale runoff typology. Developing these surveys by hand would be too resource intensive, and so far, remote sensing (de Alwis et al., 2007) has proved impractical for widespread applications. Therefore, at present, surface topography and SSURGO soil maps (the most detailed soils data are provided by the NRCS; see USDA, 2007) remain the most robust means for managing soil and water in the northeastern USA. A more concerted effort should be made, however, to better integrate differences in runoff typology (particularly lateral preferential flow paths) into VSA models and to explore new measurement techniques for increasing the resolution of soil and topography input data.

Conclusions

The VSA concepts proposed more than 40 yr ago (e.g., Betson, 1964 and Dunne and Black, 1970) for northeastern watersheds have been subject to few updates and improvements. However, there is a growing body of literature from areas with coevolved glacial soils (e.g., Soulsby and Tetzlaff, 2008) suggesting that differences in the lateral and vertical redistribution of water (runoff typology) can increase the contributions of hillside features on overall watershed functioning. Therefore, we more closely considered the effects of the lateral redistribution of water via saturation-excess overland flow in a 2.51-km² watershed using hydrometric, chemical, and isotopic data. The intensive spatial surveys revealed that hillsides have saturation areas that were maintained by spring heads and connected to the stream via overland flow in larger rain events. These results were supported by hydrometric measurements, which showed a rapid response of overland flow paths and transient near-stream surface saturation during the events. Finally, hydrograph separations using isotope and geochemicals confirmed that shallow overland flow supplies up to 59% of peak streamflow and event water (water from the most recent rainfall event) contributed during the falling portion of the stream hydrograph.

The spatial extent of hillside saturation areas was different than predictions from conventional VSA models. This is probable because of a lack of resolution in the input data and an inadequate consideration of lateral preferential flow paths in the structure of the VSA models. The presence of lateral preferential flow paths appeared to cause water to be transported more quickly and from sources further from the stream channel than current VSA theories would predict. The results of this study do not preclude the use of conventional VSA models for management purposes, but they do imply that for these models to “get the right answers for the right reasons,” more validation of the lateral redistribution of water resulting from preferential flow paths is required in northeastern U.S. watersheds.

References

- Ambroise, B., K.J. Beven, and J. Freer. 1996. Toward a generalization of the TOPMODEL concepts: Topographic indices of hydrological similarity. *Water Resour. Res.* 32:2135–2145.
- Betson, R.P. 1964. Water is watershed runoff? *J. Geophys. Res.* 69:1541–1552.
- Beven, K., and J. Feyen. 2002. The future of distributed modeling. *Hydrolog. Processes* 16:169–172.
- Beven, K., and M.J. Kirkby. 1979. A physically based variable contributing area model of basin hydrology. *Hydrolog. Sci. Bull.* 24:43–69.
- Bishop, K.H., H. Grip, and A. O'Neill. 1990. The origins of acid runoff in a hillslope during storm events. *J. Hydrol.* 116:35–61.
- Brown, V.A., J.J. McDonnell, D.A. Burns, and C. Kendall. 1999. The role of event water, a rapid shallow flow component, and catchment size in summer stormflow. *J. Hydrol.* 217:171–190.
- Burns, D.A., J.J. McDonnell, R.P. Hooper, N.E. Peters, J.E. Freer, C. Kendall, and K. Beven. 2001. Quantifying contributions to storm runoff through end-member mixing analysis and hydrologic measurements at the Panoche Mountain Research Watershed (California, USA). *Hydrolog. Processes* 15:1903–1924.

- Burns, D.A., P.S. Murdoch, G.B. Lawrence, and R.L. Michel. 1998. The effect of groundwater springs on NO_3^- concentrations during summer in Catskill Mountain streams. *Water Resour. Res.* 34:1987–1996.
- Buttle, J.M. 2006. Mapping first-order controls on streamflow from drainage basins: The T^3 template. *Hydrol. Processes* 20:3415–3422.
- Buttle, J.M., and D. Peters. 1997. Inferring hydrological processes in a temperate basin using isotopic and geochemical hydrograph separation a re-evaluation. *Hydrol. Processes* 11:557–573.
- Christopherson, N., and R.P. Hooper. 1992. Multivariate analysis of stream water chemical data: The use of principal components analysis for the end-member mixing problem. *Water Resour. Res.* 28:99–107.
- Dahlke, H.E., Z.M. Easton, D.R. Fuka, S.W. Lyon, and T.S. Steenhuis. 2009. Modeling variable source area dynamics in a CEAP watershed. *Ecohydrology* 2:337–349.
- de Alwis, D.A., Z.M. Easton, H.E. Dahlke, W.D. Philpot, and T.S. Steenhuis. 2007. Unsupervised classification of saturated areas using a time series of remotely sensed images. *Hydrol. Earth Syst. Sci.* 11:1609–1620.
- Dunne, T., and R.D. Black. 1970. Partial area contributions to storm runoff in a small New England watershed. *Water Resour. Res.* 6:1296–1311.
- Dunne, T., T.R. Moore, and C.H. Taylor. 1975. Recognition and prediction of runoff-producing zones in humid regions. *Hydrol. Sci. Bull.* 20:305–327.
- Engman, E.T. 1974. Partial area hydrology and its application to water resources. *Water Resour. Bull.* 10:512–521.
- Eshleman, K.N., J.S. Pollard, and A.N. O'Brien. 1993. Determination of contributing areas for saturation overland flow from chemical hydrograph separations. *Water Resour. Res.* 29:3577–3587.
- Fiebig, D.M., M.A. Lock, and C. Neal. 1990. Soil water in the riparian zone as a source of carbon for a headwater stream. *J. Hydrol.* 116:217–237.
- Gehre, M., R. Hoebling, P. Kowski, and G. Strauch. 1996. Sample preparation device for quantitative hydrogen isotope analysis using chromium metal. *Anal. Chem.* 68:4414–4417.
- Genereux, D.P. 1998. Quantifying uncertainty in tracer-based hydrograph separations. *Water Resour. Res.* 34:915–919.
- Hewlett, J.D., and A.R. Hibbert. 1967. Factors affecting the response of small watersheds to precipitation in humid regions. p. 275–290. In W.E. Sopper and H.W. Lull (ed.) *Forest hydrology*. Pergamon Press, Oxford.
- HRachowitz, M., C. Soulsby, D. Tetzlaff, J.C. Dawson, S.M. Dunn, and I.A. Malcolm. 2009. Using longer-term data sets to understand transit times in contrasting headwater catchments. *J. Hydrol.* 367:237–248.
- Inamdar, S.P., and M.J. Mitchell. 2007. Contributions of riparian and hillslope waters to storm runoff across multiple catchments and storm events in a glaciated forested watershed. *J. Hydrol.* 341:116–130.
- Kendall, K.A., J.B. Shanley, and J.J. McDonnell. 1999. A hydrometric and geochemical approach to test the transmissivity feedback hypothesis during snowmelt. *J. Hydrol.* 219:188–205.
- Kirchner, J.W., X.H. Feng, and C. Neal. 2000. Fractal stream chemistry and its implications for contaminant transport in catchments. *Nature* 403:524–527.
- Kurdish, M. 2002. *Catskill forests*. Purple Mountain Press, Fleischmanns, NY.
- Lin, H. 2006. Temporal stability of soil moisture spatial pattern and subsurface preferential flow pathways in the Shale Hill catchment. *Vadose Zone J.* 5:317–340.
- Lin, H.S., and X.B. Zhou. 2008. Evidence of subsurface preferential flow using soil hydrologic monitoring in the Shale Hills catchment. *Eur. J. Soil Sci.* 59:34–49.
- Lyon, S.W., A.J. Lembo, M.T. Walter, and T.S. Steenhuis. 2006a. Defining probability of saturation with indicator kriging on hard and soft data. *Adv. Water Resour.* 29:181–193.
- Lyon, S.W., J. Seibert, A.J. Lembo, M.T. Walter, and T.S. Steenhuis. 2006b. Geostatistical investigation into the temporal evolution of spatial structure in a shallow water table. *Hydrol. Earth Syst. Sci.* 10:113–125.
- Lyon, S.W., M.T. Walter, P. Gerard-Marchant, and T.S. Steenhuis. 2004. Using a topographic index to distribute variable source area runoff predicted with the SCS curve-number equation. *Hydrol. Processes* 18:2757–2771.
- McDonnell, J.J., M. Sivapalan, K. Vache, S. Dunn, G. Grant, R. Haggerty, C. Hinz, R. Hooper, J. Kirchner, M.L. Roderick, J. Selker, and M. Weiler. 2007. Moving beyond heterogeneity and process complexity: A new vision for watershed hydrology. *Water Resour. Res.* 43:W07301.
- McDowell, W.H., and S.G. Fisher. 1976. Autumnal processing of dissolved organic matter in a small woodland stream ecosystem. *Ecology* 57:561–569.
- McGlynn, B.L., J.J. McDonnell, J. Seibert, and C. Kendall. 2004. Scale effects on headwater catchment runoff timing, flow sources, and groundwater-streamflow relations. *Water Resour. Res.* 40:W07504.
- McGuire, K.J., J.J. McDonnell, M. Weiler, C. Kendall, B.L. McGlynn, J.M. Welker, and J. Seibert. 2005. The role of topography on catchment-scale water residence time. *Water Resour. Res.* 41:W05002.
- Mehta, V.K., M.T. Walter, E.S. Brooks, T.S. Steenhuis, M.F. Walter, M. Johnson, J. Boll, and D. Thongs. 2004. Application of SMR to modeling watersheds in the Catskill Mountains. *Environ. Model. Assess.* 9:77–89.
- Moore, T. 1989. Dynamics of dissolved organic carbon in forested and disturbed catchments, Westland, New Zealand, 1. Māimai. *Water Resour. Res.* 25:1321–1330.
- Reynolds, R.J. 2000. Hydrogeology of the Beaver Kill Basin in Sullivan, Delaware, and Ulster Counties, NY. USGS Water-Resources Report 00-4034. Troy, NY.
- Rich, J.L. 1934. Glacial geology of the Catskills. *New York State Museum Bull.* 299. University of the State of New York, Albany, NY.
- Sklash, M.G., and R.N. Farvolden. 1979. The role of groundwater in storm runoff. *J. Hydrol.* 43:45–65.
- Soren, J. 1963. The ground-water resources of Delaware County, New York. *New York State Department of Conservation Bulletin GW-50*.
- Soulsby, C., and D. Tetzlaff. 2008. Towards simple approaches for mean residence time estimation in ungauged basins using tracers and soil distributions. *J. Hydrol.* 363:60–74.
- Soulsby, C., D. Tetzlaff, S.M. Dunn, and S. Waldron. 2006. Scaling up and out in runoff process understanding: Insights from nested experimental catchment studies. *Hydrol. Processes* 20:2461–2465.
- Steenhuis, T.S., M. Winchell, J. Rossing, J.A. Zollweg, and M.F. Walter. 1995. SCS runoff equation revisited for variable source runoff areas. *J. Irrig. Drain. Eng.* 121:234–238.
- Tetzlaff, D., J. Seibert, and C. Soulsby. 2009. Inter-catchment comparison to assess the influence of topography and soils on catchment transit times in a geomorphologic province; the Cairngorm Mountains, Scotland. *Hydrol. Processes* 23:1874–1886.
- Troch, P.A., G.A. Carillo, I. Heidbuchel, S. Rajagopal, M. Switanek, T.H.M. Volkmar, and M. Yeager. 2008. Dealing with landscape heterogeneity in watershed hydrology: A review of recent progress toward new hydrological theory. *Geogr. Compass.* 3:375–392.
- Tromp-van Meerveld, H.J., and J.J. McDonnell. 2006. Threshold relations in subsurface stormflow 1. A 147 storm analysis of the Panola hillslope. *Water Resour. Res.* 42:W02410.
- USDA. 2007. *Soil survey of Delaware County, New York*. NRCS, Washington, DC.
- Waddington, J.M., N.T. Roulet, and A.R. Hill. 1993. Runoff mechanism in a forest groundwater discharge wetland. *J. Hydrol.* 147:37–60.
- Walter, M.T., V.K. Mehta, A.M. Marrone, J. Boll, T.S. Steenhuis, M.F. Walter, and C.A. Scott. 2002. A simple estimation of the prevalence of Hortonian flow in the New York City watersheds. *J. Hydrol. Eng.* 10:169–170.
- Wels, C., R.J. Cornett, and B.D. LaZerte. 1991. Hydrograph separation: A comparison of geochemical and isotopic tracers. *J. Hydrol.* 122:253–274.
- West, A.J., S.E. Findlay, D.A. Burns, K.C. Weathers, and G.M. Lovett. 2004. Catchment-scale variation in the nitrate concentrations of groundwater seeps in the Catskill Mountains, New York, U.S.A. *Water Air Soil Pollut.* 132:389–400.